

1. Introduction

The primary focus of modern stellar populations research is the understanding of the formation and evolution of galaxies within the context of the large-scale structure of the expanding universe. One way to approach the problem is to observe ensembles of galaxies forming and evolving as a function of redshift, or lookback time; another is to study the star-forming histories of entire galaxies from their resolved individual stars. Both methods have complementary strengths. In the high redshift approach, cosmology provides precise ages and lookback time provides a snapshot of galaxy dynamics. However, studies are limited to regions within galaxies that have high surface brightness, the properties of which must be inferred from the integrated light of the stars contained within; the most recent stellar generation dominates the observed light in any given galaxy. In the second approach, the theory of stellar evolution is applied directly to the measured temperatures and luminosities of individual stars, providing masses, ages, and abundances of stars formed over the whole history of the galaxy; however, the dynamical history of the stars is, in some cases, entirely scrambled, measurements of the ages of the oldest stars are less precise than in the high redshift approach, and only in nearby galaxies may the stars be resolved.

Existing ground-based telescopes and the Hubble Space Telescope (HST) have made substantial progress towards piecing together the formation histories of galaxies, following both of the approaches outlined above. In particular, the Hubble Deep Fields (Williams et al. 1996, 2000; Casertano et al. 2000) have revealed galaxies in various stages of assembly out to $z \sim 5$, with spatial resolution sufficient to observe their morphologies and to estimate the stellar content of their components from integrated light. HST in combination with ground-based telescopes have also studied the resolved stellar content of nearby dwarf galaxies, revealing a wide variety of star formation and chemical enrichment histories, many of which are punctuated by bursts. However, the galaxies most readily available for study of their resolved stellar content are generally too faint to observe at high redshift. Counterparts to the brighter Local Group dwarfs may have been observed in the HDF (Phillips et al. 1997), but the overlap between objects observed in integrated light at high redshift and resolved at zero redshift remains very small.

The GSMT (Giant Segmented Mirror Telescope), with the leap in angular resolution and light gathering power that it offers, will produce such overlap between the high redshift and resolved star approaches to studying galaxies that a much better picture of their formation is certain to come into view. Here, we outline the kinds of resolved stellar populations work that will be enabled by GSMT, and describe the impact these studies may have. We are particularly interested in addressing the following questions:

- What are the star formation histories of spiral bulges and disks?
- Are there visible signs of past mergers in the star formation histories of elliptical galaxies?
- Was the epoch of first globular cluster formation universal?

2. Techniques for studying stellar populations

Basic information (temperatures, luminosities, compositions) about stellar populations may be derived from broadband photometry and spectroscopy, from which we may also measure velocities for dynamical studies. Photometry is used to produce color-magnitude diagrams (CMDs) for direct comparison with predictions of stellar evolutionary theory, which are a function of stellar age, composition, and mass function. Traditionally, stellar astrophysicists have used optical bands for comparison with theoretical models, as the peak of the blackbody spectrum of the majority of stars lies in the optical. While the GSMT’s MCAO system will operate only in the infrared, it is now well known that infrared photometry is a useful alternative to optical photometry for all stellar types, and particularly for cool stars; for very dusty regions, infrared photometry is absolutely essential. For detailed abundance measurements and kinematics, spectroscopy of individual stars is necessary. The near-infrared contains a number of wavelength regions which are useful for detailed abundance analyses.

Since the middle of the 20th century, CMDs of star clusters have been used as a straightforward way to compare theoretical stellar evolutionary models with observations. Once the distance, reddening, and abundance of a cluster are known, comparison with model isochrones yields the cluster age from the absolute magnitude of the main sequence turnoff. For globular clusters, the fitting of isochrones to CMDs in this fashion has established them as some of the oldest objects in the universe. To date, crowding has precluded measuring ages of globular clusters in this fashion beyond a distance of ~ 50 kpc. In the next section, we explore the performance of the GSMT for the study of globular clusters in M31 and beyond.

The analysis of field stars is less straightforward than for star clusters. Field stars contain a mix of stellar populations which cannot be represented by any single model isochrone, but are instead a superposition of evolutionary tracks of a wide range in age, mass, and chemical composition. Recently, however, robust techniques have been developed for extracting the ages, abundances, and even distances, reddenings, and mass functions from field star CMDs. In the following section, we use such a technique, which is based on the work of Dolphin (1997), to evaluate the capability of the GSMT for measuring star formation histories in galaxies beyond the Milky Way.

Much of the work that we aim to do with GSMT relies on our ability to perform accurate photometry with the planned MCAO system. We thus include a discussion on the expected accuracy of MCAO photometry in the next section.

3. Surveying Nearby Galaxies with GSMT

3.1. M32

M32 is a common benchmark for population synthesis studies of more distant elliptical galaxies, and thus will be an important target for the GSMT. Integrated spectroscopy combined with

population synthesis analyses conclude that the inner region of M32 is intermediate ($\sim 4\text{--}5$ Gyr) in age and has solar metallicity (Trager et al. 2000, del Burgo et al. 2001). Davidge et al. (2000) observed the central $20''$ of M32 with Gemini North and Hokupa'a, and detected AGB stars to $M_K \sim -5$. While the $\sim 0''.12$ resolution of their images was insufficient to test whether the population synthesis models are correct, they established that there are no radial trends in the luminous AGB population within the inner $20''$.

3.1.1. Crowded-field MCAO photometry

Olsen, Blum, & Rigaut (2003; hereafter OBR) evaluated the performance of GSMT in a $20''$ simulated field centered on the core of M32. They found that crowding, rather than the noise from photon statistics, is the limiting factor for the accuracy and depth of photometry in this region of high surface brightness. Thus, evaluating the ability to do crowded-field photometry with the GSMT's MCAO system is very important for the stellar populations science case.

Figure 1 shows the DAOPHOT/ALLSTAR CMD derived from OBR's simulated GSMT images of M32. These images were produced from an artificial stellar population drawn from Girardi et al. (2000; hereafter G00) isochrones and representing a star formation history of 3% 1 Gyr ($[\text{Fe}/\text{H}] = 0$), 35% 5 Gyr ($[\text{Fe}/\text{H}] = 0$), and 62% 10 Gyr ($[\text{Fe}/\text{H}] = -0.3$) stars. The PSFs used to place the stars in the simulated images are described in detail by OBR. Briefly, the PSFs have diffraction-limited cores with FWHM of $0''.009$ in J and $0''.015$ in K , with Strehl ratios of 0.2 in J and 0.6 in K . They do *not* vary as a function of position in the frame. Figure 1 shows that in this somewhat idealized case, we are able to easily distinguish the three input sequences in the recovered CMD of the core of M32.

Because a realistic MCAO system will contain some variation in Strehl ratio as a function of position, following the work of OBR we performed simulations incorporating a variable Strehl PSF. These PSFs were generated by Brent Ellerbroek, and have Strehl ratios that decrease from $\sim 85\%$ to $\sim 80\%$ from center to edge in K and from $\sim 62\%$ to $\sim 50\%$ in J . Figure 2 (top left) shows the CMD produced using DAOPHOT/ALLSTAR and a constant PSF model. As expected from the variable Strehl, the scatter in color of the bright stars is $\sim 5\%$ (compare with Figure 1). In order to remove the effect of the variable Strehl, we need to be able to measure the contribution of the PSF halo light as a function of position in the frame using aperture photometry. The standard procedure for doing this is to identify a handful of bright stars in the field, subtract the companion stars using the PSF model, and perform aperture photometry on the subtracted image. Figure 3 shows that this is practically impossible to do in the crowded fields of interest for the GSMT. While the PSF model does an excellent job of subtracting the cores of neighboring stars, the large radius of the apertures within which the light must be measured contains contributions from a prohibitively large number of contaminating PSF halos. However, if the Strehl ratios may be predicted from the wavefront sensor output (Ellerbroek, personal communication), then 1% photometry of bright stars may be possible (Figure 2, top right). Figure 2 (bottom left) shows that the spatial resolution

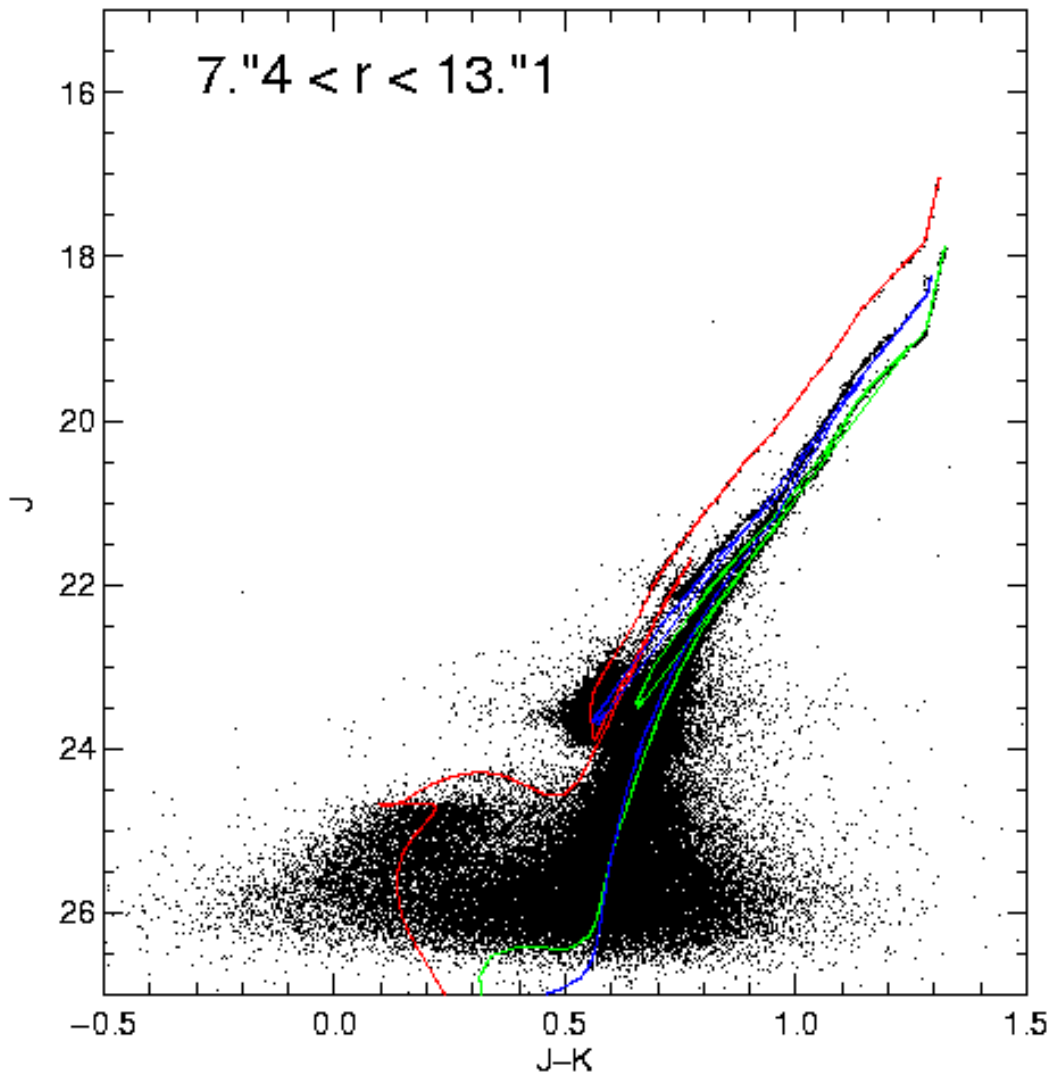


Fig. 1.— Simulated GSMT CMD of a region near the center of M32. The PSFs used to produce the artificial JK images have diffraction-limited cores with FWHM $0''.009$ (J) and $0''.015$ (K); the Strehl ratios are 0.2 (J) and 0.6 (K), and are uniform across the field.

of the Strehl ratio prediction need not be large, because the Strehl is a slowly varying function of position. The Strehl ratio prediction would also be extremely valuable for the absolute calibration of the photometry, which places even greater demands on knowledge of the halo contribution to the PSF than $\sim 1\%$ relative photometry.

3.1.2. *The star formation and chemical enrichment history of M32*

The CMD shown in Fig. 1 contains a superposition of three distinct stellar populations. We explored the ability of GSMT data to recover these populations using Olsen’s (1999) implementation of the method described by Dolphin (1997), with some modifications. In brief, we constructed a set of model CMDs from the G00 isochrones, with one model each for 15 different age bins and 3 different metallicities, for a total of 45 independent models. We assumed zero reddening and a distance modulus of 24.3 to M32, as used in constructing the input population. We used the isochrones and a Salpeter IMF to produce Hess diagram representations of each model, which we then convolved with the photometric errors. Rather than use the photometric errors derived directly from the simulations, which in practice is time-consuming, we used the analytically predicted crowding errors of OBR. We then produced a Hess diagram of the Fig. 1 CMD at identical resolution to the set of 45 models.

We used the *Numerical Recipes* (Press et al. 1992) routine *amoeba* and the Poisson maximum likelihood parameter (Dolphin 2002) to find the linear combination of the 45 models that provides the highest chance of representing the parent population of the simulated CMD. In performing the solution, we only used the portion of the Hess diagram for which OBR predict that the completeness is $\sim 100\%$, which for the M32 CMD is $J < 25$. Figure 4 (left) shows the input population box (cf. Hodge 1989) used to represent M32, and Figure 4 (right) the population box derived from the simulating CMD using the maximum likelihood method. We find that we closely recover the relative fractions to within a few percent, ages, and metallicities of the input population, with $\lesssim 0.5$ Gyr accuracy in age for ages up to 5 Gyr, ~ 1 Gyr age accuracy at 12 Gyr, and $\lesssim 0.3$ dex accuracy in metallicity. Although our analysis is somewhat idealized by our use of the G00 isochrones to both produce the input model and derive the solution, the derived random errors should be accurate.

Figure 5 shows the population box that results from using a simulated 8-m NGST CMD in place of the GSMT CMD. While the three input populations are still distinguishable, the errors in age and metallicity are much larger. Indeed, from the NGST CMD it is impossible to distinguish between star formation that occurs in rapid bursts and star formation that continues for several Gyr.

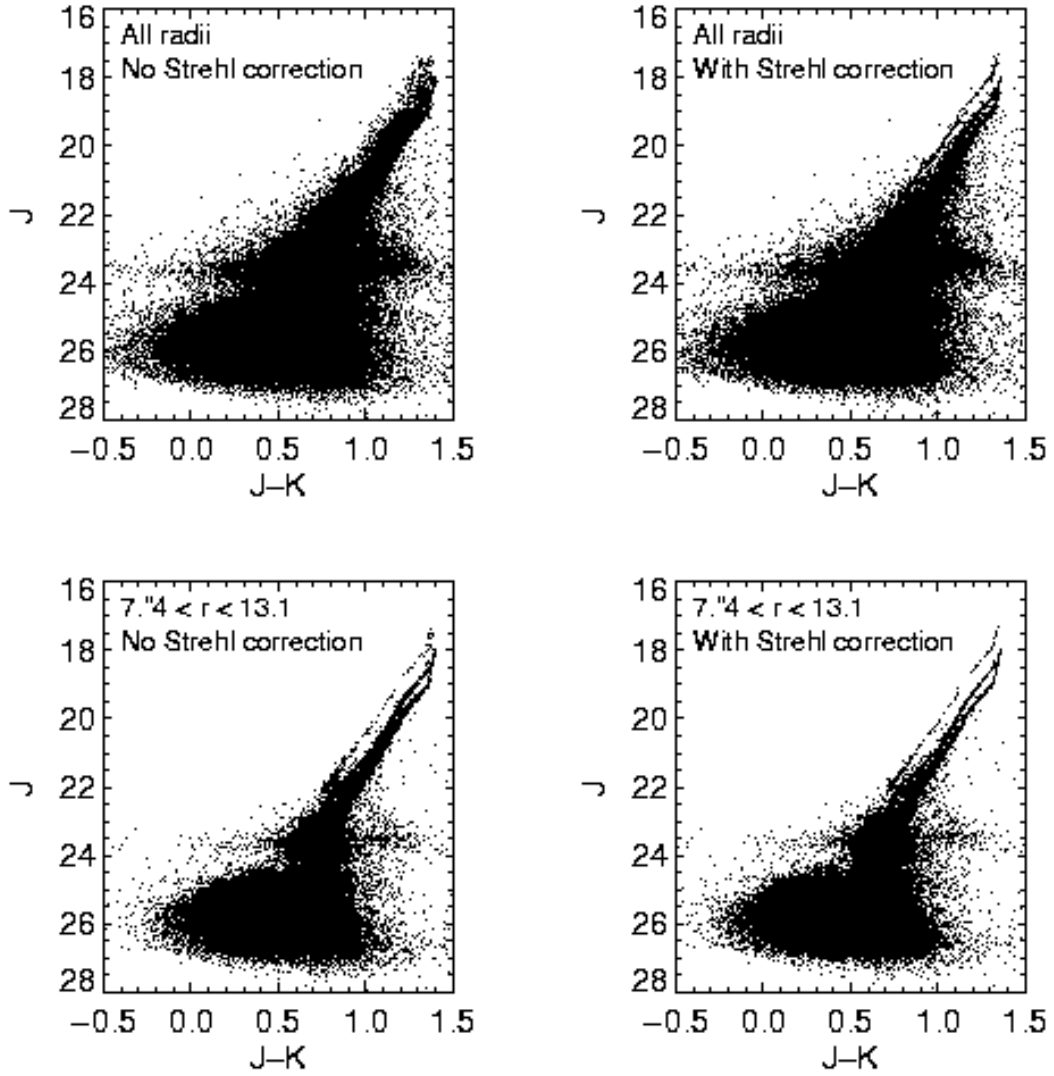


Fig. 2.— Top left: M32 CMD from simulation produced with a GSMT PSF having smoothly varying Strehl. A uniform PSF model was used to produce the photometry. All stars from the $20'' \times 20''$ simulated image are included. Top right: M32 CMD including all simulated stars, after correcting for the variable Strehl. Bottom left: Same as top left, but only for stars within the annulus $7''.4 < r < 13''.1$ centered on M32. Bottom right: Same as bottom left after correction for variable Strehl.

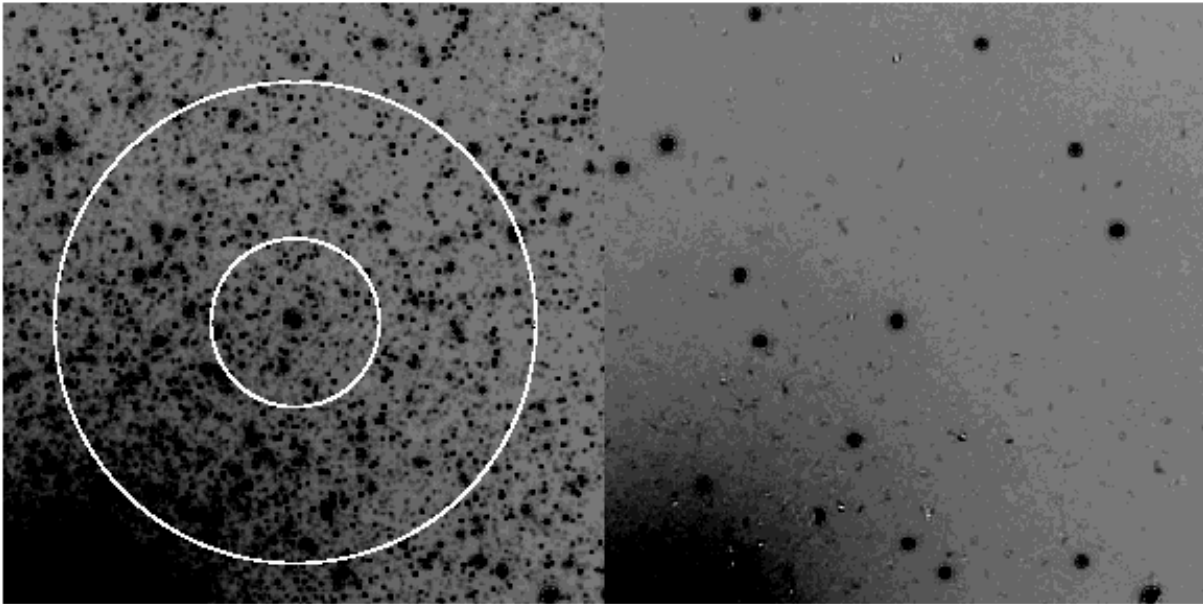


Fig. 3.— Original (left) and PSF-subtracted (right) sections of the simulated M32 K image containing variable Strehl; bright stars used to define the PSF have been left untouched in the subtracted image. The small white circle shows the radius out to which aperture photometry must be performed in order to produce 2% relative photometry across the entire image. The large circle shows the radius containing 95% of the light from the star; thus, for 5% absolute photometry, aperture corrections out to at least this radius are necessary. While the PSF cores subtract nicely, the background light is dominated by the overlapping halos from the entire ensemble of stars, not by the PSF halos of the select bright stars.

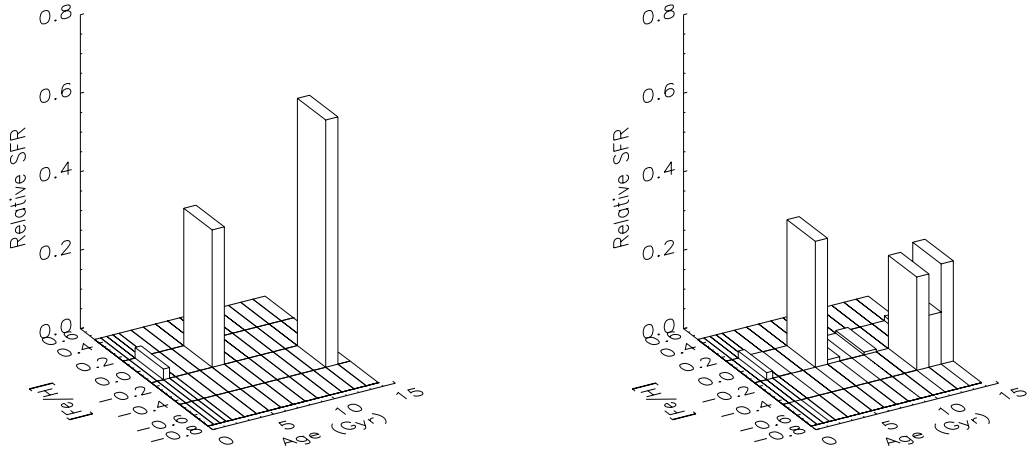


Fig. 4.— Left: input population box (cf. Hodge 1989) for the M32 simulation. Right: Population box recovered from the simulated CMD shown in Fig. 1 using the maximum likelihood technique described in the text.

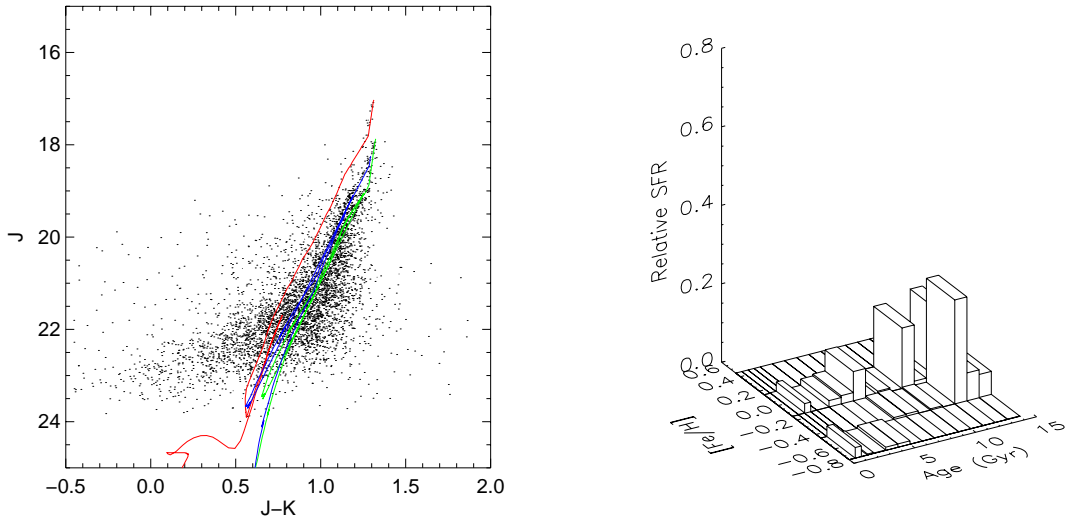


Fig. 5.— Simulated M32 measurements with NGST. Left: the CMD derived for the annulus $7''.4 \leq r \leq 13''.1$ centered on M32 is shown compared with the input isochrones. The PSF used to produce the artificial images was assumed a diffraction-limited 8-m telescope, with FWHMs of $0''.032$ (J) and $0''.057$ (K). Right: Population box derived from the CMD on the left.

3.1.3. A GSMT survey of M32

The goals for a GSMT survey of M32 would be to characterize the age and abundance of the dominant stellar population and to look for population gradients with radius from the center. We would measure the star formation and chemical enrichment histories from CMDs taken at a sample of three radii from the center, using spectroscopy of ~ 100 bright red giants per field to verify the abundances. The following table lists the surface brightnesses of three possible pointings, the magnitude at which crowding limits photometry to 10% accuracy, the imaging time needed to reach the crowding limit, and the time needed to complete the spectroscopy.

3.2. The M31 bulge

The ages of the predominant stellar populations in spiral bulges and disks are basic constraints on disk galaxy formation. While studies of the integrated light of spiral bulges and disks clearly suggest that the majority of bulges are older than disks (e.g. Abraham et al. 1999), it is well-established that a small population of young stars drastically affects integrated colors (cf. Ellis et al. 2001); measuring the star formation histories of bulges and disks directly from their resolved stellar populations is thus extremely important. In addition, the chemical enrichment histories of bulges and disks provide an important link to the evolution of the gas component of galaxies; such detailed information is unavailable for systems outside the Milky Way.

The bulge of M31, the closest large spiral galaxy to our own, is both an important target for GSMT and a testbed for our ability to extract the star formation and chemical enrichment histories of nearby spiral galaxies, such as the members of the Sculptor and M81 groups. Following the procedure used for M32 above, we created an artificial stellar population for the effective radius of the M31 bulge ($\Sigma_K \sim 17.5$ mags arcsec $^{-2}$; Kent 1983) by using the G00 isochrones and an assumed mix of 5% 1 Gyr ([Fe/H]=0.0) stars, 20% 5 Gyr ([Fe/H]=0.0) stars, and 75% 13 Gyr ([Fe/H]=-0.6) stars, roughly following the star formation and chemical abundance distribution of the Galactic center (van Loon et al. 2003, Blum et al. 2003). We also assumed a reddening of $A_K = 0.024$ (Han 1996) and differential reddening of 0.005 in A_K . We then placed these stars in artificial J and K images using the model GSMT MCAO PSF and an assumed exposure time of 10,000 seconds distributed over 100 exposures. We used a uniform Strehl PSF for these images, as we assume that the wavefront sensor information may be used to correct for any Strehl variation and supply the absolute photometric calibration. Figure 6 shows the resulting CMD, along with the input model isochrones.

As for the M32 case, we constructed a set of model CMDs from the G00 isochrones, with 45 independent models spanning ages from 0.5 – 13 Gyr and [Fe/H] from -0.6 to 0.0. We assumed reddening $A_K = 0.024$, a distance modulus of 24.3, and a Salpeter IMF; we did not include any differential reddening in the models. We used the OBR analytical predictions to estimate the photometric errors due to crowding, and restricted ourselves to $M_J < 2.0$, fainter than which

completeness is less than 100%. Our images inadvertently saturated at the bright end, so we also restricted the models to $M_J > -4.8$. Figure 7 shows both the input and recovered population boxes for the M31 bulge. We find that the GSMT will have excellent ability to recover the star formation and chemical enrichment history of the M31 bulge, with similar accuracy in age and metallicity as for M32, and a few percent accuracy in the recovered star formation rates. Because the M31 disk has surface brightness similar to that of the bulge effective radius, we expect similar sensitivity to recovering the disk populations, as long as the regions of highest reddening are avoided. Of course, in the optical, bulk and differential reddening would be of substantially greater concern than in the near-infrared.

3.2.1. Surveying M31 with the GSMT

The goals for a GSMT survey of M31 would be to compare the relative ages and abundances of the dominant stellar populations in the bulge and disk, for comparison with the predictions of models of disk galaxy formation. We would measure the star formation and chemical enrichment histories from CMDs taken in one bulge field and one disk field, using spectroscopy of ~ 100 bright red giants per field to verify the abundances and measure abundance patterns. The following table lists the surface brightnesses of two possible pointings, the magnitude at which crowding limits photometry to 10% accuracy, the imaging time needed to reach the crowding limit, and the time needed to complete the spectroscopy.

3.3. The Giant elliptical galaxy NGC 3379

Comparing the star formation histories of giant elliptical galaxies with those of disk galaxies places another valuable constraint on models of galaxy formation (cf. Ellis et al. 2001). Elliptical galaxies are popularly thought to be produced through the merger of disk galaxies, the signatures of which should be detectable in the star formation and chemical enrichment histories of ellipticals. The bimodal color distributions seen in the globular cluster systems of many elliptical galaxies (e.g. Geisler et al. 1996) are often used to argue that globular clusters form in mergers (Ashman & Sefc 1992); if correct, then spectacular population signatures must lie hidden in the field stars.

At a distance modulus of ~ 30.44 (Salaris & Cassisi 1999), NGC 3379 is one of the most accessible giant elliptical galaxies. Following the procedures described above, we produced simulated JK images of a field taken at the effective radius ($1'$) of NGC 3379, performed photometry on the images, and solved for the star formation and chemical enrichment history represented by the CMD. The surface brightness at the effective radius of NGC 3379 is $\Sigma_K \sim 17.0$ mags arcsec $^{-2}$, which we modelled with a stellar mix identical to that used for the M31 bulge. Figure 8 shows the CMD we obtained from the simulated images alongside the recovered population box. We find that the photometry is 100% complete to just below the level of the red giant branch tip, such that the

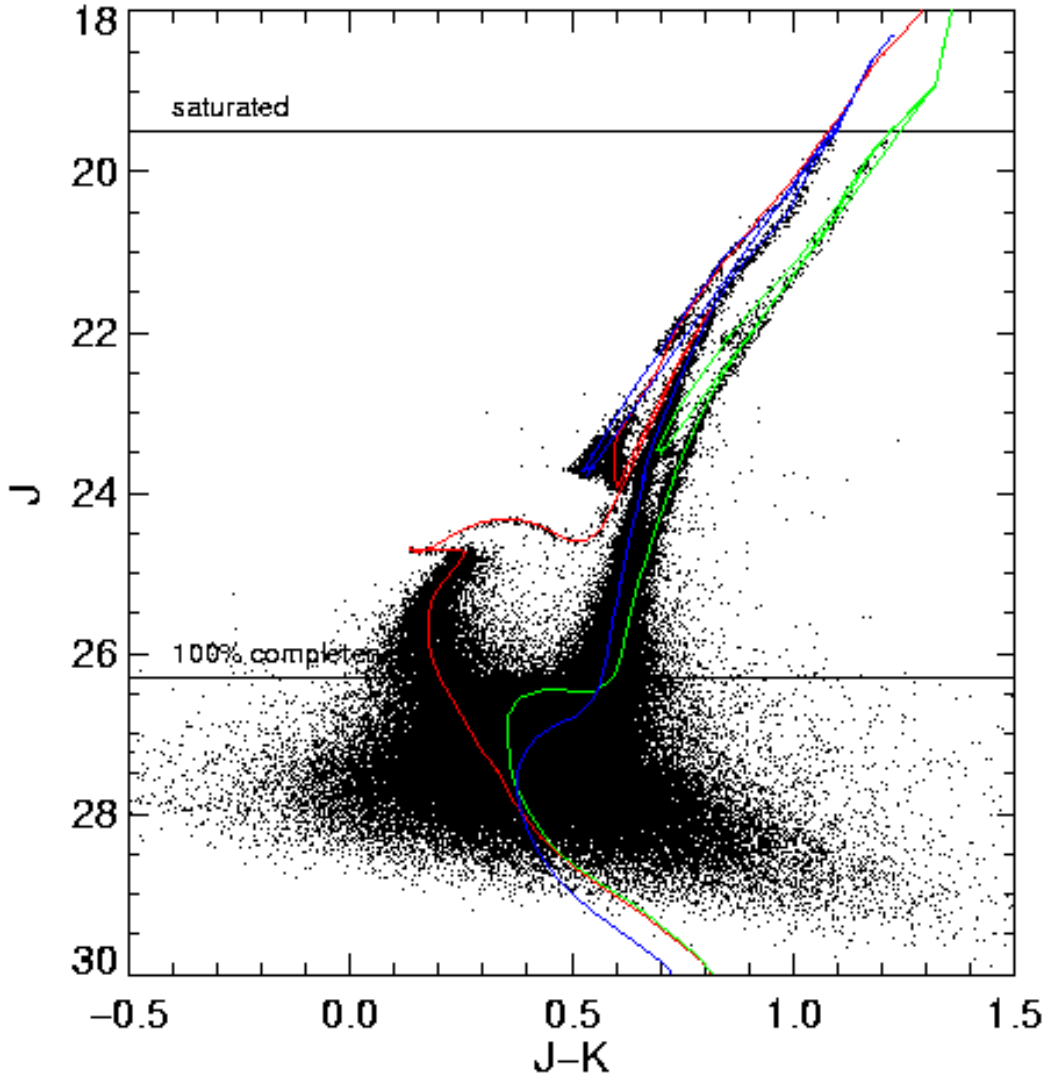


Fig. 6.— Simulated GSMT of a field at the effective radius ($\sim 18'$) of the M31 bulge, which has surface brightness $\Sigma_K \sim 17.5$. The input populations used in the simulation are a mix of 5% 1 Gyr ($[\text{Fe}/\text{H}]=0.0$) stars, 20% 5 Gyr ($[\text{Fe}/\text{H}]=0.0$) stars, and 75% 13 Gyr ($[\text{Fe}/\text{H}]=-0.6$) stars. A uniform Strehl PSF was used to create the images. The horizontal lines show the saturation limit for a 100-second exposure and the 100% completeness limit.

asymptotic giant branch contains most of the population information. The output population box recovers the three distinct populations, but with errors of at least $\sim 1\text{--}2$ Gyr in age and $\gtrsim 0.3$ dex in metallicity. However, as the typical suggested metallicity differences between globular cluster populations in elliptical galaxies is ~ 1 dex, the age and metallicity resolution of GSMT for elliptical galaxies should be adequate to identify the products of possible past mergers.

3.3.1. The NGC 3379 GSMT survey

The goals for a GSMT survey of NGC 3379 would be to look for the signatures of past mergers in the star formation and chemical enrichment histories of a select number of fields, and to measure the kinematics of any indentified sub-populations. Three pointings taken at different radii would provide an excellent start for the CMD analysis, while velocities of ~ 100 stars per sub-population would allow us to investigate differences in kinematic properties. The following table lists the surface brightnesses of three possible pointings, the magnitude at which crowding limits photometry to 10% accuracy, the imaging time needed to reach the crowding limit, and the time needed to complete the spectroscopy.

3.4. Globular clusters in M31 and beyond

The old ages and long survival times of globular clusters make them excellent tools for the study of the formation and evolutionary histories of galaxies. There are many ways by which the globular cluster systems of giant galaxies could have assembled. Giant elliptical galaxies may build up their systems in galaxy mergers through the combination of the progenitor systems (e.g. Forbes et al. 2000) and through the formation of new clusters in the merger (e.g. Schweizer et al. 1996). Galaxies such as the Milky Way and M31 likely formed many of their clusters *in situ*, perhaps in the hierarchical collapse of the halo (Côté et al. 2000). Parts of GC systems may also have been built through the accretion of the clusters of dwarf galaxies (Côté et al. 1998). Indeed, the Sagittarius dwarf is falling into the Milky Way (Ibata et al. 1994), in the process contributing ~ 4 GCs to the halo (Da Costa & Armandroff 1995).

Ages, abundances, and kinematics provide the primary clues by which we may learn how globular cluster systems form. While globular cluster velocities are accurately obtained with current ground-based telescopes out to distances including the Virgo cluster, their ages and metallicities must be estimated from uncertain modelling of integrated colors and spectra. Ages and metallicities from resolved stars are difficult to measure beyond ~ 100 kpc because of crowding. An important goal for stellar population research with the GSMT will thus be producing CMDs and spectra for globular cluster stars in M31 and beyond.

Following the procedures outlined above, we produced an artificial globular cluster population drawn from a 12 Gyr $[\text{Fe}/\text{H}] = -1.5$ G00 isochrone. We assumed the cluster to be similar to the LMC

globular cluster NGC 1835, that is with a central surface brightness $\Sigma_J \sim 14.4$ mags arcsec⁻², core radius of 1.16 pc, and total luminosity of $M_J \sim -10.2$ (Olszewski et al. 1996, Mackey & Gilmore 2003). We simulated two sets of JK images, one with the cluster at an M31 distance modulus of 24.3 and the other at a Virgo cluster distance modulus of 30.9. For both image sets, we assumed a total exposure time per filter of 10,000 seconds distributed over 1000 exposures.

Figure 9 shows the recovered CMDs of the two artificial clusters. At the distance of M31, photometry is possible to the level of main sequence turnoff. Comparison of the recovered fiducial line with model isochrones suggests that a measurement of the age to ± 2 Gyr will be possible, with the metallicity measured either from the shape of the red giant branch or from spectroscopy of individual red giant stars. At the distance of the Virgo cluster, we will no longer be able to determine ages from the resolved stars, but will be able to verify whether differences in metallicity of ~ 0.3 dex are present in the cluster systems from the color of the RGB and AGB.

3.4.1. A survey of globular cluster systems with the GSMT

The variation in Milky Way globular cluster properties with Galactocentric radius has profoundly affected our view of the Milky Way’s formation; a study of the CMDs of a sample of ~ 50 globular clusters in M31 would form the basis for a powerful comparison of the properties of the Milky Way and M31 halos. A study of the CMDs of ~ 50 globular clusters in the galaxy NGC 4472 could provide proof for the suggested bimodal metallicity distribution. The following table lists the magnitude at which crowding limits photometry to 10% accuracy for typical globular clusters and the imaging time needed to reach the crowding limit.

4. SUMMARY

The GSMT offers a tremendously exciting opportunity for the study of stellar populations. The GSMT will measure the star formation histories and chemical enrichment histories of all components of Local Group galaxies in unprecedented detail; initiate the study of resolved stars in giant elliptical galaxies; and allow the precise measurement of globular cluster ages out to M31 and abundances out to distances of the Virgo cluster. By vastly increasing the range of distances and stellar densities in which stars may be resolved, the GSMT will turn stellar populations into a powerful tool for the study of galaxy formation and evolution, in a way that complements the study of galaxies at high redshift.

Photometry of stellar populations in nearby galaxies is limited by 1) the collecting area of the telescope, through the shot noise from the observed photons; and 2) the telescope resolution, through the crowding of stars in the dense environments of interest. For the problems considered here, ground-based telescopes operating in natural seeing generally reach the crowding limit long before the photon-noise limit. Indeed, even diffraction-limited telescopes will be limited more by

crowding than photon noise. This document has explored what a 30-m GSMT can do for a few case study environments; however, it is also important to compare the capability of the 30-m with telescopes of other aperture sizes. The following table shows the magnitudes at which diffraction-limited 8-m, 20-m, and 30-m telescopes are crowding-limited in a variety of environments, and the exposure times needed to reach those magnitudes, assuming Strehl of 80% in K .

The limits imposed by crowding translate directly into our ability to recover star formation and chemical enrichment histories from near-IR color-magnitude diagrams. For example, near the center of M32, we found that the higher resolution of an MCAO-corrected GSMT over that of an 8-m NGST produces a precision more than a factor of two better in the derived star formation rates, ages of star formation bursts, *and* metallicities. In the table that follows, we summarize the results of our calculations for the other case studies. The increased capability of the 30-m for deriving astrophysical quantities from CMDs will play a deciding role for answering the questions posed in this document: **1) What are the star formation histories of spiral bulges and disks? 2) Are there visible signs of past mergers in the star formation histories of elliptical galaxies? 3) Was the epoch of first globular cluster formation universal?**

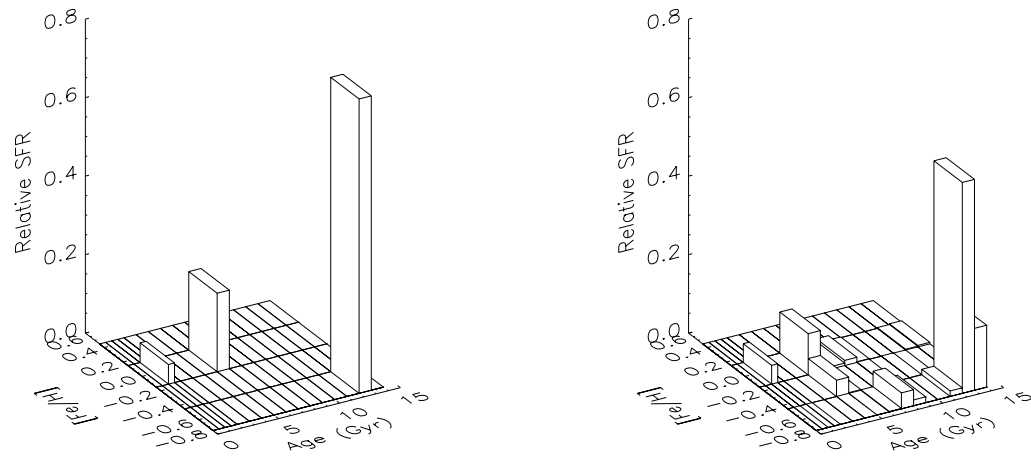


Fig. 7.— Left: Input population box used to produce CMD in Figure 6. Right: Recovered M31 population box.

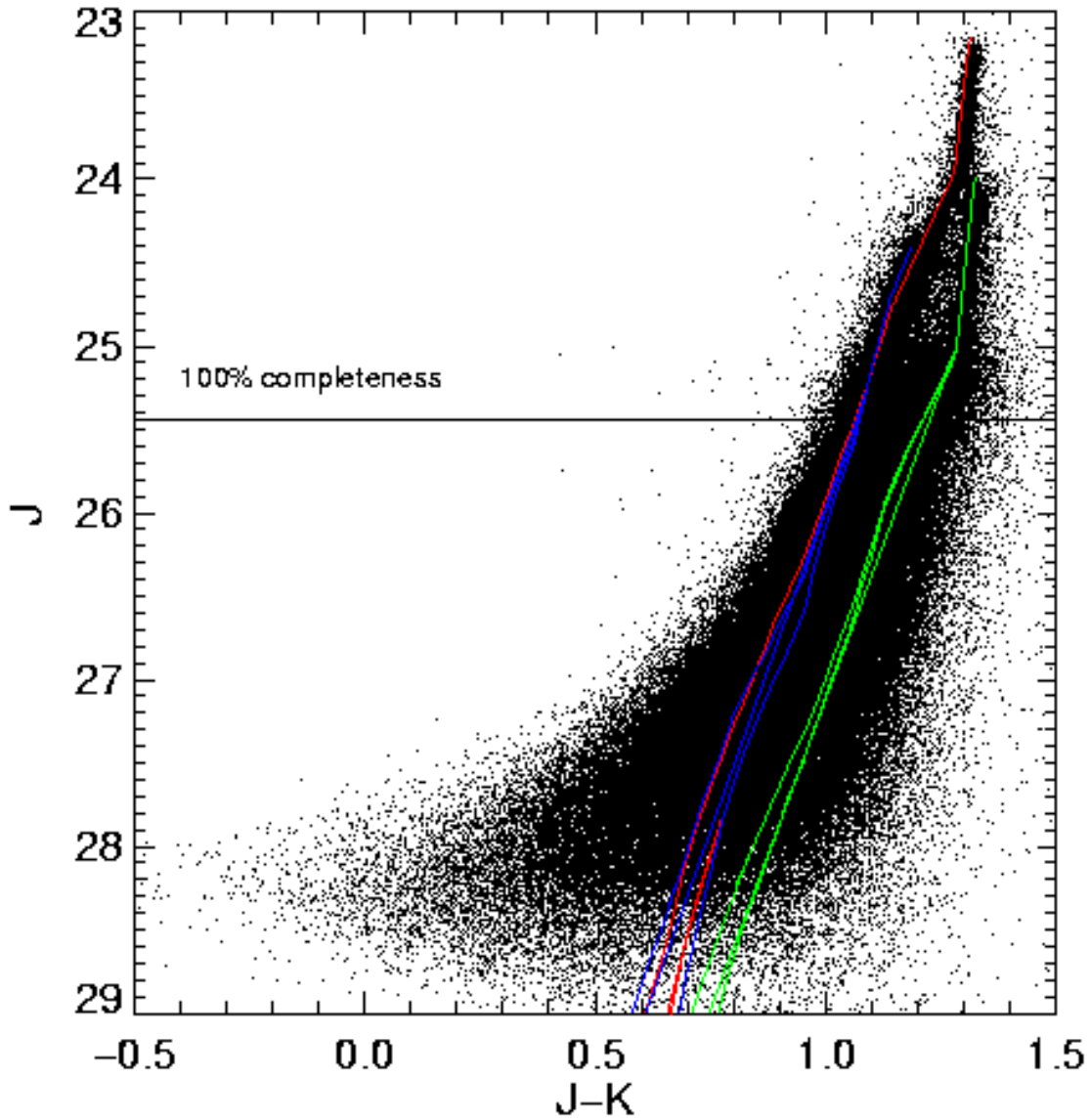


Fig. 8.— Simulated GSMT of a field at the effective radius ($\sim 1'$) of NGC 3379, which has surface brightness $\Sigma_K \sim 17.0$ mags arcsec $^{-2}$. The input populations used in the simulation are the same as used for the M31 bulge simulation. A uniform Strehl PSF was used to create the images. The horizontal line shows the 100% completeness limit.

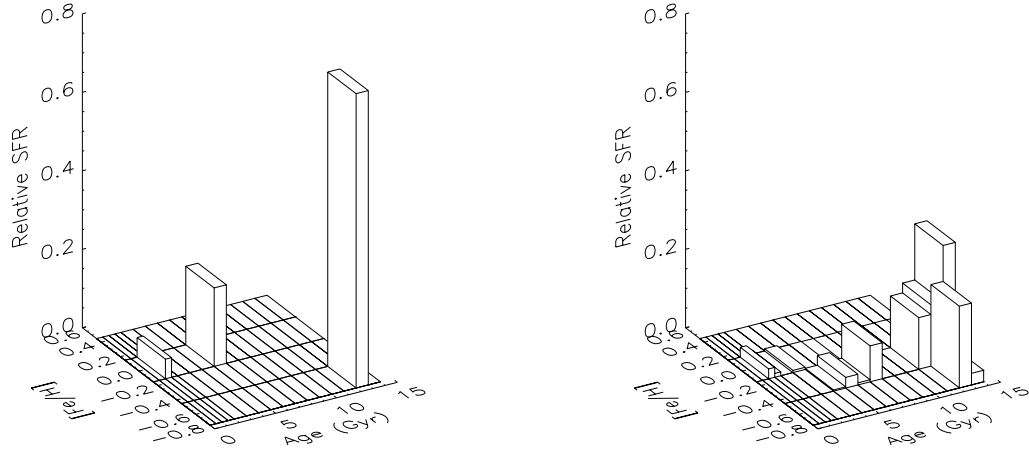


Fig. 9.— Left: Input population box used to produce CMD in Figure 8. Right: Recovered NGC 3379 population box.

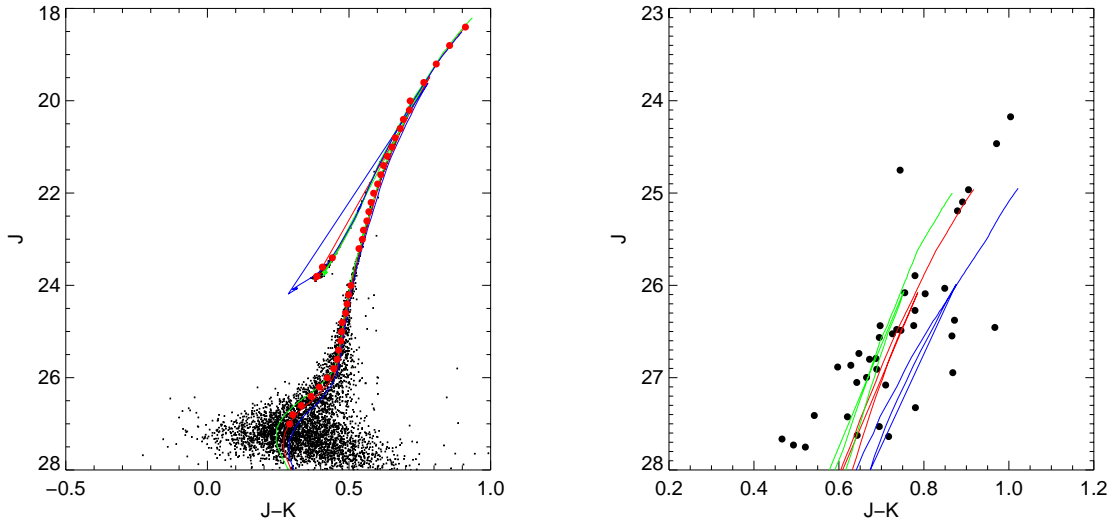


Fig. 10.— Left: A globular cluster in M31 as seen with GSMT. The isochrones drawn have $[\text{Fe}/\text{H}] = -1.5$ and ages of 10, 12, and 14 Gyr. From the photometry, it will be possible to measure the ages of such clusters with a precision of ± 2 Gyr. Right: The identical globular cluster is placed at the distance of the Virgo cluster. The isochrones drawn have ages of 12 Gyr and $[\text{Fe}/\text{H}] = -1.67, -1.5,$ and -1.2 . The photometry will allow the estimation of the cluster metallicities to an accuracy of ± 0.3 dex.